International Journal of Fracture **43**: 117–131, 1990.

Interlaminar shear fracture of laminated composites

HERZL CHAI
Polymers Division, Institute for Materials Science & Engineering, National Institute of Standards and Technology, Gaithersburg, Maryland 20899, USA

Received 1 June 1988; accepted in revised form 30 September 1989

Abstract. The interlaminar fracture toughness in mode II and mode III of a number of advanced composites was studied using beam type test specimens and scanning electron microscopy. Special emphasis was placed on elucidating the material aspects of the fracture process and on quantifying the effect of matrix on fracture energy.

The fracture energy in mode II was independent of crack extension while that for mode III exhibited a rather probablistic "resistance" behavior that was attributed to the effect of fiber bridging. The initiation fracture energy, considered here the true measure of G_{IIIC}, coincided with G_{IIC}. For either mode, the interlaminar region ahead of the crack tip exhibited considerable plastic deformations, the severity that is believed to control the laminate toughness. The interlaminar fracture energy in shear, hereby denoted as G_{SC} ($= G_{IIC} = G_{IIIC}$), was accurately predicted from a straightforward adhesive joint fracture test provided the adhesive thickness coincide with the thickness of the interlaminar resin layer.

1. Introduction

Most research to date on interlaminar fracture has focused on mode I loading, which proved to be the critical failure mode in first-generation, brittle-matrix composites. Use of tough matrix systems was shown to greatly improve composites' damage tolerance [1], but unfortunately the accompanying reduction in G_{IIC}/G_{IC} for such materials necessitates the additional consideration of shearing modes in any fracture analysis. This is manifested under cyclic loading, where threshold G_{IIC} values for tough resins may be as little as the mode I toughness of brittle epoxy resins [2, 3].

Athough research on mode II interlaminar fracture has grown considerably in the last few years [2–7], there are still a few unresolved issues concerning testing and data interpretation, the most pressing one being perhaps a meaningful interpretation for the observed nonlinearity in the load-deflection curve. Most works to date have largely ignored this effect, treating the fracture problem in accordance with linear elastic fracture mechanics. This simplification is believed to be a leading cause for the considerable scatter in reported toughness data (i.e. for T300/BP-907*: 1300–1950 N/m[3]; for AS4/PEEK: 1765 N/m[2], 1800–2500[6]). Another issue of prime implication concerns the effect of hackles or microcracking in the resin-rich interlaminar region on fracture toughness. It is generally believed [2, 7] that the additional fracture surface associated with hackles is the main cause for the nearly order of magnitude increase in G_{IIC} over G_{IC} for brittle-matrix composites. Recent mode II tests on adhesively-bonded joints [8] showed, however, that hackles or oblique microcracks may affect G_{IIC} only

* Certain commercial materials and equipment are identified in this paper in order to specify adequately the experimental procedure. In no case does such identification imply recommendation or endorsement by the National Institute of Standards and Technology, nor does it imply necessarily the best available for the purpose.

marginally, the latter was dominated by plastic deformations in the interlayer. Another controversial issue concerns the dependence of G_{IIC} on crack extension, Δa. While the general consensus is that G_{IIC} is independent of Δa, tests on a double-cracked lap-shear specimen [5] produced a resistance behavior, with the fracture energy at onset of unstable crack growth being nearly twice that at the beginning of damage growth.

The case of mode III seems even more cumbersome. There appears to be no sound testing methodology for this fracture mode, and the limited data that are available show considerable scatter. Utilizing a double-cracked-flexure specimen [9], the mode III interlaminar fracture energy of a number of unidirectional composites was shown to display a "resistance" behavior, the effect that was attributed to the development of damage behind the crack tip characterized by loose fiber bundles bridging the opposing crack faces. An initiation and a plateau value for G_{IIIC} were identified corresponding, respectively, to the first instant of damage growth and the instant when the damage zone at the crack tip became fully-developed (i.e. when G_{IIIC} became independent of Δa). The initiation value was as little as the neat resin G_{IC} while the plateau value exceeded the initiation by a factor of 10 to 30, being about twice as large as G_{IIC}. A similar G_{IIIC}/G_{IIC} ratio (~ 2) was also reported for wood [10] or AS4/3502 composite [11], though no "resistance" behavior was noted in these studies. The validity of these findings is questionable, however, in light of recent results from mode II and mode III fracture tests on adhesively-bonded joints [8]. Utilizing testing concepts similar to those reported herein for composites, it was found that the adhesive fracture energies in mode II and mode III were indistinguishable, a coincidence that held true for all three different adhesive systems tested and, for a given material, irrespective of bond thickness.

Interlaminar fracture testing of composites is a tedious, time-consuming and expensive undertaking. Moreover, new resin candidates for improved damage tolerance are often available only in small quantities. Although it is generally recognized that the interlaminar fracture toughness is dominated by the matrix phase, it is of practical importance to determine that relationship quantitatively. An earlier study [12] showed that the composites' G_{IC} could be accurately predicted by testing the matrix *in situ* as an adhesive bond. Such correlation was possible only when the bondline thickness was made sufficiently small, on the one hand, and the composites' toughness was determined at the initial instant of crack growth, on the other hand. Similar observations were also made in [13]. (It can be argued, of course, that interlaminar crack growth in actual composite parts may be a prolonged process associated with extensive fiber-bridging, in which case the apparent fracture toughness may well exceed the initiation toughness. Analysis of such failure is difficult, however, and the applicability of classical fracture mechanics concepts to such situations is not well substantiated). The purpose of the present work is to extend the above composite-joint toughness correlation into the shearing modes. The first phase of this effort will attempt to provide a sound characterization for interlaminar shear fracture in laminated composites. The results from this phase will then be used to determine quantitatively the role of the matrix constituent on laminate toughness. The latter task was made possible from recent fracture tests on adhesive joints which determined G_{IIC} and G_{IIIC} for bondline thicknesses as small as that of the interlaminar resin layer of laminated composites. The test variables in this study were resin ductility, orientation of the delaminating plies and crack extension.

2. Experimental

2.1. Fabrication

As shown in Fig. 1, the mode II and mode III specimens used are variants of the popular mode I DCB configuration, with the particular fracture mode being affected by the manner of loading. These tests, each of which provides a continuous type crack growth, have been originally designed for mode II [14] or mode III [10] testing of wood. It should be noted that the finite width of this mode III specimen (which is dictated by practical considerations) should lead to some mode II stresses near the intersection of the crack plane and the free-edges of the specimen. The effect of this imperfection on the measured G_{IIIC} will be discussed at the end of this report. The particular choices of a relatively large beam height, h, and a nearly quasi-isotropic layup (Fig. 1c) were made, respectively, to prevent large deformations of the cracked beams in applications to tough composites and to minimize the considerable transverse shear deformations present in the commonly-employed unidirectional layup; the effect of this on G_{II} is controversial.

As was the case for mode I [12], the three composites studied were AS4/3502, AS4/BP-907 and AS4/PEEK (APC2). The first two matrix constituents are amorphous thermosetting resins while PEEK is a semi-crystalline thermoplastic. Also, the H3502 resin is brittle while BP-907 and PEEK exhibit a nonlinear stress-strain behavior. The test specimens were cut to the dimensions shown in Fig. 1 from panels that were fabricated from commercially available prepreg tapes per manufacturer recommendations. The layup (Fig. 1c) consisted of 62 plies, the first 30 in each split arm are quasi-isotropic. An initial crack was formed prior to curing by inserting a 25 μm thick Kapton film (AS4/3502, AS4/BP-907) or aluminum foil (AS4/PEEK) between the central $-\theta$ and $+\theta$ layers. The value of θ was selected as (Table 1) 0, 30, and 60 deg. (AS4/3502) or, due to material shortage, only 0 and 60 for AS4/BP-907 and 0 and 30 for AS4/PEEK.

The initial crack length was approximately 40 and 100 mm in mode II and III, respectively. The corresponding ratio of crack length, a, to half-span, $L(a/L)$ for the mode II specimen

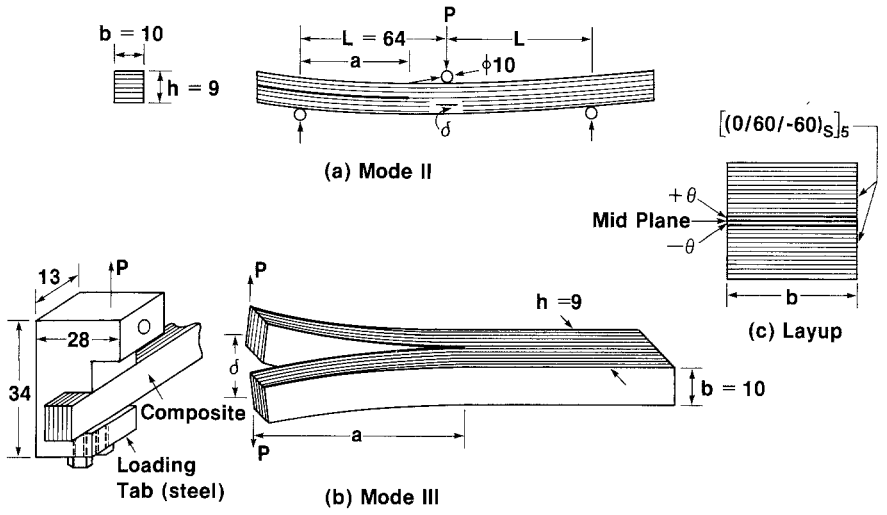

Fig. 1. Interlaminar shear fracture test specimens. All dimensions are in mm.

of over 0.6 insured that, under fixed grip conditions, G_{II} was a decreasing function of crack length. To generate natural crack, prior to testing, the debond was extended approximately 1 mm from the insert border by means of carefully wedging open the crack tip [12]. Crack tip visibility was enhanced by painting the observed edge of the specimen with a white corrective fluid. A prescaled paper strip was attached along the crack line to aid in determining the instantaneous crack tip position.

2.2. Testing

The specimens were loaded at a crosshead speed of 0.51 mm/min (mode II) or 2.5 mm/min (mode III) in a closed-loop servohydraulic testing machine (MTS) operated in a stroke control mode. Load P and load-deflection δ were traced on a chart recorder. The mode II deflection was monitored with an extensometer (Instron). The latter was mounted directly under the loading pin so as to circumvent the non-negligible effect of machine deformation. Figure 2 exemplifies loading histories for several mode II and mode III fracture tests pertaining to composites (a, b) and adhesive joints (c, d); the latter tests were generated in [8] using test configurations and data reduction procedures similar to those applied in this work.

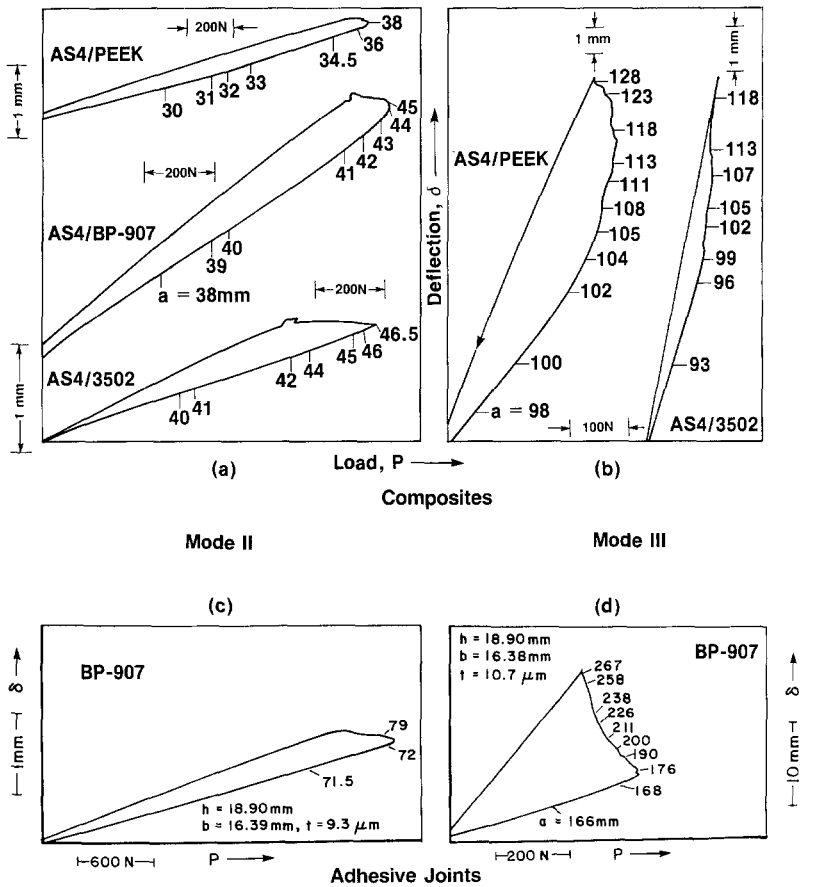

Fig. 2. Loading histories for composites (a,b) and adhesive joints (c,d) [8] in mode II and mode III. Tic marks indicate crack length.

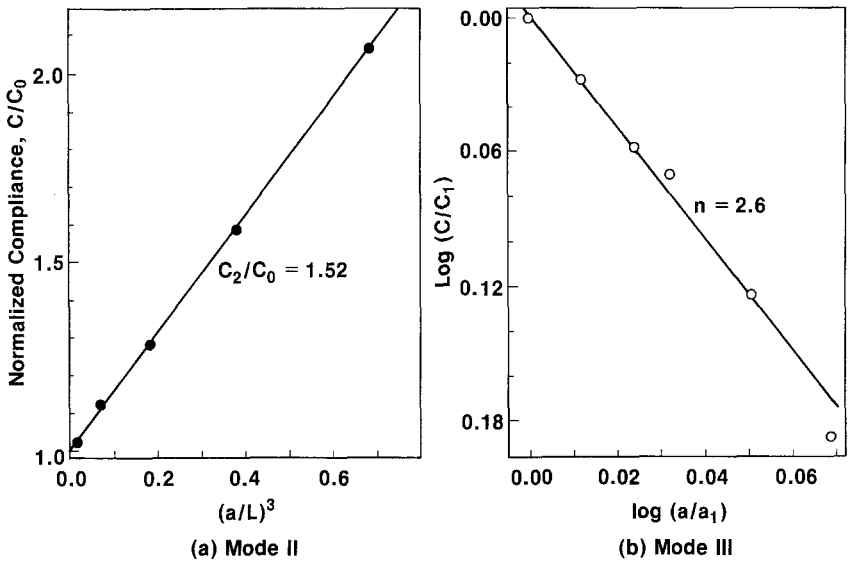

Fig. 3. Compliance plot for the AS4/3502(a) and AS4/PEEK(b) composites detailed in Fig. 2a and 2b, respectively. a_1 is the crack length at which data reduction began.

The tic marks on the chart in this figure indicate instantaneous crack length. This was established visually (mode III) or using an X20 traveling microscope (mode II).

All loading traces in Figs. 2a, b exhibit a nonlinear behavior similar to their adhesive counterparts in Figs. 2c, d. This effect, which is more pronounced for the ductile matrix systems, was due to irreversible resin deformation at the crack tip region, not a gross plastic deformation of the test specimens. After completion of each mode II test, the specimen was shifted horizontally on its support, and a new test carried out. In this way as many as three tests could be done on a single specimen.

For each individual test a compliance plot was generated, see Fig. 3. In this and all subsequent figures, filled and open symbols denote mode II and mode III fracture, respectively. The data for these plots were either taken from the fracture test (mode III) or generated separately prior to testing (mode II). In the latter case, the applied load was only a fraction of the peak load. Figure 3 shows that the compliance, C, in each mode could be well fitted by a straight line such that

$$C_{\mathrm{II}} = c_0 + c_2 (a/L)^3, \quad C_{\mathrm{III}} = c_3 a^n \tag{1}$$

where c_0, c_2, c_3 and n are experimentally determinable constants. The energy release rates were calculated from the compliance method [8]:

$$G_{\mathrm{II}} = \frac{1.5\, c_2 (aP)^2}{bL^3}, \quad G_{\mathrm{III}} = \frac{c_3 n}{2b} P^2 a^{n-1} = \frac{n}{2b} \frac{P\delta}{a} \tag{2}$$

where b is the beam width. The experimental values for c_2/c_0 and n were typically 1.3–1.7 and 2.5–3.0, respectively. The corresponding beam theory predictions are 1.5 and 3.0.

Calculation of fracture energy necessitates the elucidation of the critical conditions from (2). It was found in the analogous study on adhesive joints that these conditions prevail once

the peak load on the P-δ curve is reached (see Figs. 2c, d); thereafter the fracture energy was independent of crack length [8]. It was suggested that the peak load corresponds to the instant of full development of the plastic deformation zone at the crack tip or the start of self-similar crack growth [8]. Consequently, the peak load and its corresponding crack length, a_1, were used in (2) to calculate G_{IIC} or G_{IIIC}. This is in contrast to common practice employing the initial crack length, a_0, in conjunction with peak load for calculating G_{IIC} [2–4, 6–7]. Figure 2a shows that the relative difference between these two values becomes considerable for the highly ductile PEEK. In the case of mode III (Fig. 2b), the occurrence of peak load is seen to be obscured by a continuous increase in P. This behavior, which differs from the bonded joint case (Fig. 2d) where the load decreases monotonically following the peak load, is believed to result from the development of an additional damage zone characterized by fiber-bridging. Nevertheless, the P-δ traces from Fig. 2b (or similar tests) seem to show a distinguishable slope change starting at $a = 99$ mm (AS4/3502) or at $a = 105$ mm (AS4/PEEK). It is proposed that this event signifies the maturity of the plastic zone, and thus the critical conditions for crack growth. The corresponding G_{IIIC} shall be termed "initial". It is emphasized that this definition differs from [9] (or [5], in the case of mode II) where "initiation" was identified merely with the start of damage formation.

3. Results and discussion

Following testings, all specimens were split open and the fractured surface classified using a stereo-optical microscope as either interlaminar (i.e. planar, no loose fibers) or otherwise intralaminar (i.e. failure outside the interlaminar plane). As shown in Table 1, of the 42 tests conducted, 8 mode II and 11 mode III specimens produced the latter failure which is of no current interest, the majority occurring for the case where the plies above or below the delaminating plane are orientated off the beam axis ("off-axis interface"). This, however, may be partially due to edge effects introduced by beam width finiteness. (Note the lack of lateral edges for a truly anti-plane stress field or for the practical case of embedded delamination should thus enhance the likelihood of incurring interlaminar as opposed to intralaminar failure in such situations.) Nevertheless, the available data are believed sufficient for a meaningful characterization of interlaminar shear fracture.

3.1. Test results

Table 1 summarizes the fracture data pertaining to a truly interlaminar failure. The mode II fracture energy was independent of crack extension. The G_{IIC} value for the 0/0 interface, AS4/3502, of 590 N/m is similar to the values generally quoted for similar brittle-matrix composites. For the highly ductile PEEK, the present value (2315 N/m) well exceeds the value of 1765 given in [2]. This may be partially due to use in [2] of the initial crack length, a_0, as opposed to the concurrent value (a_1) pertaining to the peak load that was employed in this work. As indicated from Fig. 2a, the ratio a_1/a_0 for AS4/PEEK is substantially greater than 1 (i.e. 38/30), which would amount to over 60 percent increase in the reported G_{IIC} (see Eqn. (2)). It is interesting to note that the present value of G_{IIC} for AS4/BP-907 (2325 N/m) is over twice that obtained most recently by the author in testing of ASTM

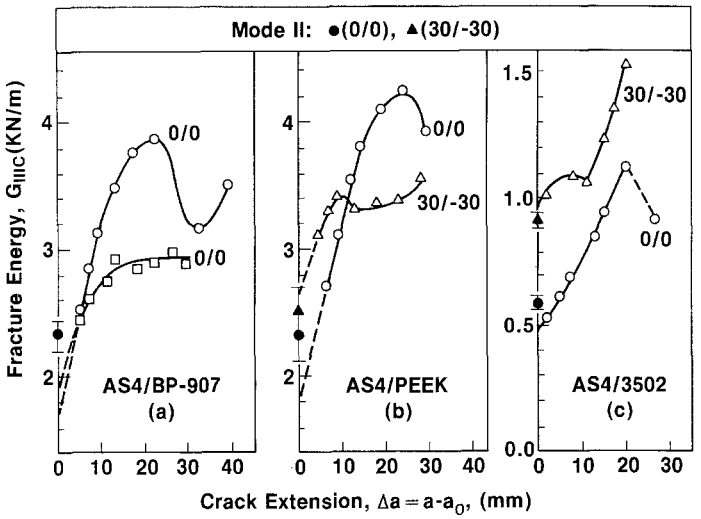

Fig. 4. Mode III fracture energy (open symbols) as a function of crack extension (a_0 is the initial crack length) for various materials and various delaminating interfaces. Solid symbols denote mode II fracture values. Straight line connecting data points indicate a slip-stick type crack growth.

Round-Robin specimens. As will be argued in a later section, however, this particularly large scatter for AS4/BP-907 as well as the larger toughness values for the off-axis interfaces as compared to the 0/0 from Table 1 (i.e. about 8 percent for AS4/PEEK and 40 percent for AS4/3502) is probably due to a thickness difference of the interlaminar resin layer.

The fracture behavior for mode III is exemplified in Fig. 4 (open symbols) for all materials and layups. In all cases the fracture energy exhibits a "resistance" behavior which resulted from the development of a damage zone characterized by detached fibers bridging the delaminating interfaces. The initial rise is followed by a leveling off starting at a certain value of Δa which defines the length of the fiber-bridging zone. As can be deduced from Fig. 4, this length is typically several times the length of the plastic zone inasmuch as the latter is determined by the peak load or the first data point on the "resistance" curve. As is particularly apparent from Fig. 4a which depicts results from two repeating tests, except for the initiation value the "R"-curve characteristics are quite probablistic, the disparity includes the extent of the fiber-bridging zone, plateau level and specific behavior within the plateau range. These occasional toughness variations may be attributed to an apparently random process of breakage of fiber bundles bridging the crack faces. It has been shown in the analogous mode I study that the "resistance" curve may also depend on the orientation of plies above and below the delaminating interfaces [13, 15] as well as on beam thickness [9, 12], the effects that greatly diminish its significance. Analogously to the mode I case, it is proposed here that the initiation fracture toughness is the true measure of G_{IIIC}. (Note: an alternative G_{IIIC} value can be obtained by extrapolation of the "R"-curve to $\Delta a = 0$. This produces an "asymptotic" value that may be viewed as an "idealized" fracture toughness in which the energy lost to fiber bridging during the evolution phase of the plastic zone is subtracted from the initiation value.)

Figure 4 shows that the value of G_{IIIC} thus defined agree well with its mode II counterpart (solid symbol) for each material and each ply orientation, a trend which is consistent with that found for bonded joints [8]. The apparent exception to that role reported for wood [10]

or composites [11] is likely a consequence of overlooking the initial phase of crack growth. Indeed, the reported G_{IIC} for AS4/3502 [11] (1200 N/m) is similar to that for large crack extension in Fig. 4c. Furthermore, the "initiation" values in [9] which are considerably smaller than their mode II counterparts are also believed to be misleading because they were derived from the first appearance of damage at the crack tip. As could be deduced from the tic marks on the P-δ curves in Figs. 2b and 2d, that event occurs well before the commencement of a self-similar, stable type crack growth. Similar argument can also be made with respect to the initial mode II fracture toughness values given in [5, 6].

3.2. Morphology

Figure 5 exemplifies the morphology for the 0/0 interface. The viewing spots in these prints are at the center of the fractured surface, and they correspond to the peak load, which is believed to signify the onset of stable, self-similar crack growth. The fracture surface for the brittle system (upper prints) in either mode is flat, mostly confined to the resin phase. (Although some fiber breakage is evident, its contribution to the total fracture work is deemed minor.) This contrasts sharply with the rich pattern of inclined microcracks or hackles that are generally reported for mode II [2, 7], see an example in Fig. 6a. These microcracks, which are typically oriented at 45 deg. to the long axis of the beam, are generally attributed to the presence of a tensile stress component in the resin rich regions between plies or individual fibers; the tensile stress is also maximized at 45 deg. to the beam axis. The photo micrograph shown in Fig. 6a was obtained from a region on the fracture surface that was well ahead of that corresponding to the peak load. As evident from the drastic slope change following the peak load in the P-δ curves of Fig. 2a, AS4/3502, in this range the crack speed was relatively large. Apparently, the associated higher deformation rate at the crack tip caused the matrix to behave in a more brittle fashion, which enhanced tensile microcracking. Because no attempt was apparently made in [2, 7] to distinguish between the initial and the rapid damage growth phases, it is possible that the hackle morphology in those works reflects rapid rather than the desired stable crack propagation. The morphological differentiation above is important because the increased free surface associated with hackles is widely held responsible for the nearly order of magnitude increase in G_{IIC} as compared to G_{IC}. However, the lack of surface roughness (or dense hackle population) for AS4/3502 (Fig. 5) clearly rules out such an argument in favor of plastic deformations. This reasoning is also supported from the morphology of the adhesive joint test which is duplicated in Fig. 8. The adhesive used in fabricating this joint was the same as the matrix used in the above composite, and the bond thickness was comparable to the interlaminar resin thickness. As shown, the fracture of this highly cross-linked, brittle adhesive is characterized by extensive plastic deformations or material distortion. Moreover, the corresponding adhesive fracture energy (~ 700 N/m, Fig. 9) is comparable to that of the AS4/3502 composite, yet only little microcracking is evident from Fig. 8.

The off-axis interface, Fig. 6b, is richer in fracture details which are reflective of the more complex fiber-matrix interaction. A particularly interesting feature is the arrays of vertical microcracks within the interlaminar resin layer which appear alongside much finer microcracks or hackles running between individual fibers. The unique relationship between microcrack spacing and interlayer thickness found in the analogous adhesive joint test (e.g. Fig. 14 of [8]) can be used to estimate the interlaminar resin

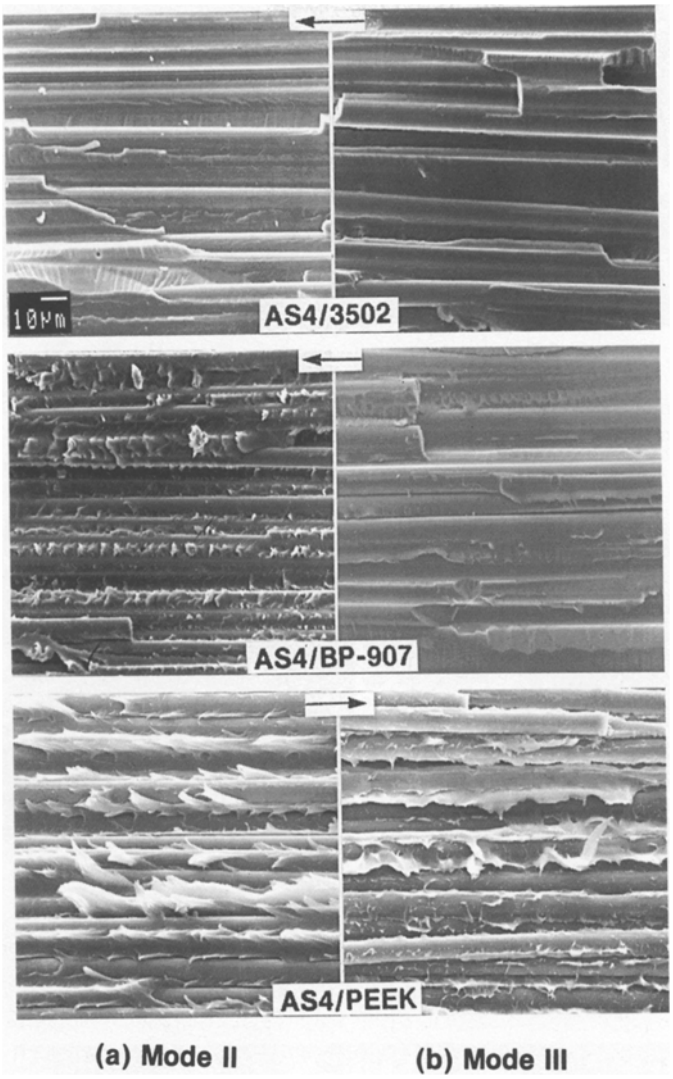

Fig. 5. Scanning electron micrographs exemplifying interlaminar fracture morphology for a continuous type crack growth, 0/0 interface. Viewing spot corresponds to peak load (mode II) or to first data point on the *R*-curve (mode III). The observed areas are at the middle of the fractured surface. Scale in upper left is common to all prints. In these and all subsequent prints, arrow indicates direction of crack growth and tilt angle = 20°.

thickness, t_r. For example, the spacing of about 14 μm evident in Fig. 6b would correspond to $t_r \sim 2.5\,\mu$m.

The morphology of the ductile matrix systems, Figs. 5 and 7, is characterized by a much greater resin deformation. This is manifested for PEEK by highly elongated texture details extending either in the shearing direction (0/0 interface, Fig. 5) or the fiber direction (30/−30, Fig. 7). The microcrack spacing in Fig. 7 seems to vary across the prints (i.e. $\sim 10\,\mu$m in upper right corner vs 20–40 μm in lower left corner in Fig. 7b), which is probably due to local thickness variation of the interlaminar resin layer. Also visible in Figs. 5 and 7 are regions of apparently bare fibers (for example, upper right in Fig. 7a and upper left or center right in Fig. 7b) which always seem to be surrounded by regions of elevated matrix.

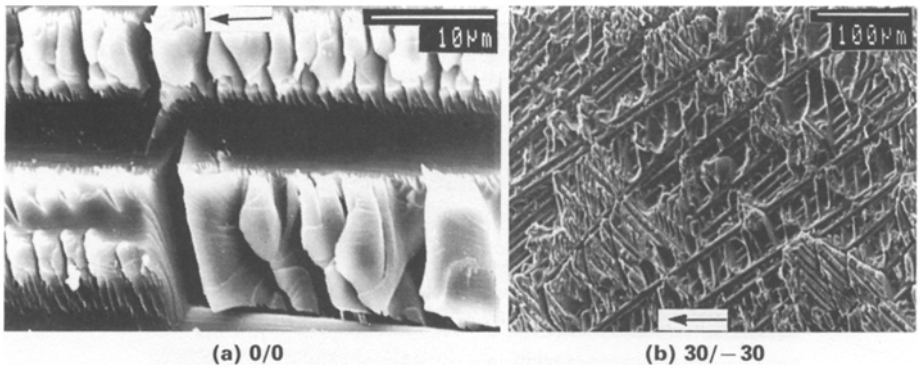

Fig. 6. Mode II interlaminar fracture surfaces for AS4/3502. Viewing spot is located about midway between peak load and the start of unloading (see Fig. 2a), where the growth is rapid (a), or at peak load (b).

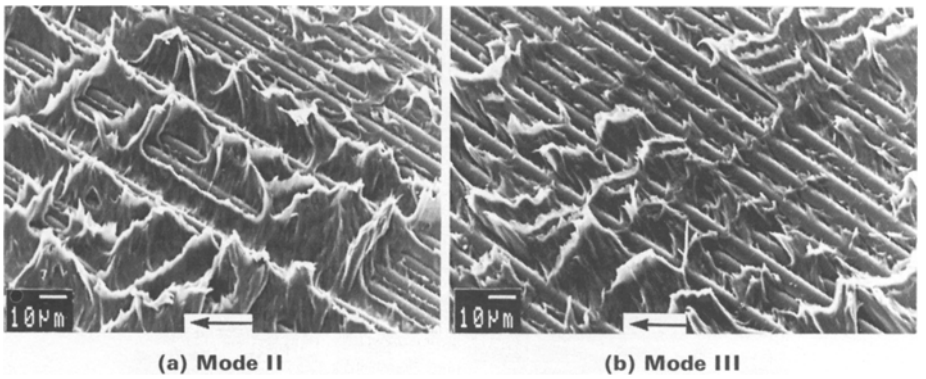

Fig. 7. Interlaminar fracture surface for AS4/PEEK, 30/−30 interface. Slow crack propagation. The observed areas are at the middle of the fractured surface.

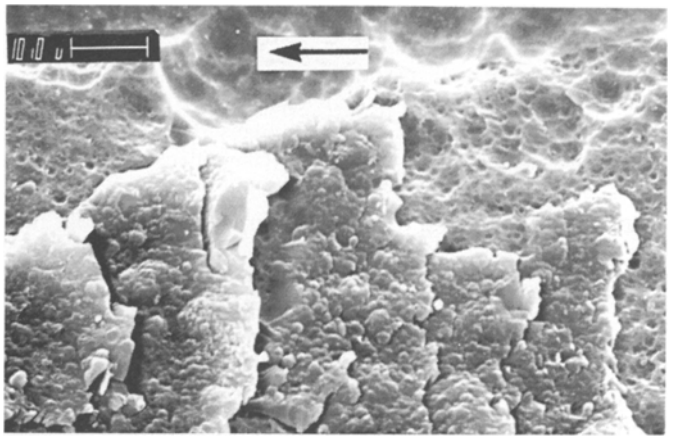

Fig. 8. Mode II fracture surface of adhesive bond showing interlayer plastic deformations and microcrackings [8]. Adhesive is H3502, a highly cross-linked, brittle epoxy. Bond thickness, $t_c = 3.3\ \mu m$. Viewing spot corresponds to peak load.

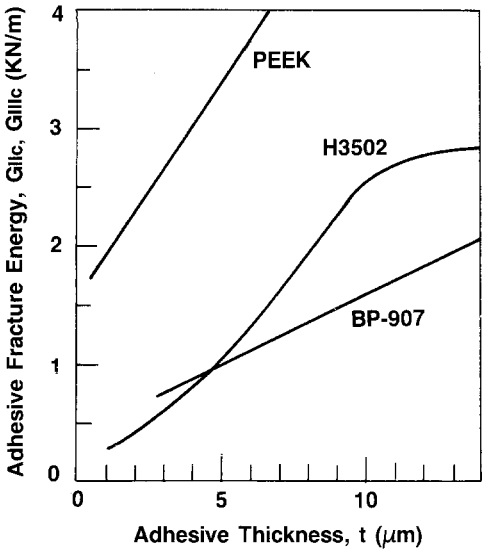

Fig. 9. Mode II and mode III adhesive fracture energy as function of bond thickness [8] for three adhesives used as matrices in the presently studied composites.

This is similar to the "island" morphology found in the study of adhesive joints which could be seen in Fig. 8 (i.e. upper right or upper left of this micrograph shows one side of the adherent/matrix interface while lower part corresponds to the opposite interface). This morphology was attributed to a mechanically-forced, near-interface linkage of neighboring tensile microcracks, not adhesion type failure.

4. Composite-joint toughness correlation

Figure 9 shows the dependence of mode II or mode III adhesive fracture energy on bond thickness [8]. Results are presented for all three resins used in fabricating the present polymer composites. In all cases, the adhesive fracture energy increases with bond thickness, a phenomenon attributed to the increase in the volume of resin undergoing plastic deformations. The great sensitivity of fracture energy to bond thickness evident in this figure dictates that the lateral dimension of the interlaminar resin layer must be accurately determined if a meaningful composite-joint correlation is desired. Figure 10 shows micrographs of polished composites sections typifying all delaminating interfaces of interest. The interlaminar region for the off-axis interfaces (b) seems well defined but that for 0/0 (a) is hardly distinguishable due to merging of adjacent 0 deg. plies. This is except for AS4/BP-907 where interlaminar resin pockets as large as several fiber diameter are quite common.

Precise quantification of the lateral dimension of the resin rich region constituting the lateral extent of the plastic zone from such micrographs is difficult to accomplish because of unknown factors such as extent of plasticity around fibers and preferred fracture path. Figure 10c describes figuratively the evaluation technique adopted. This print is identical to the upper print in Fig. 10b except for a horizontal white mask identifying our choice of the plastic deformation region. As shown, the latter was established by circling interlaminar

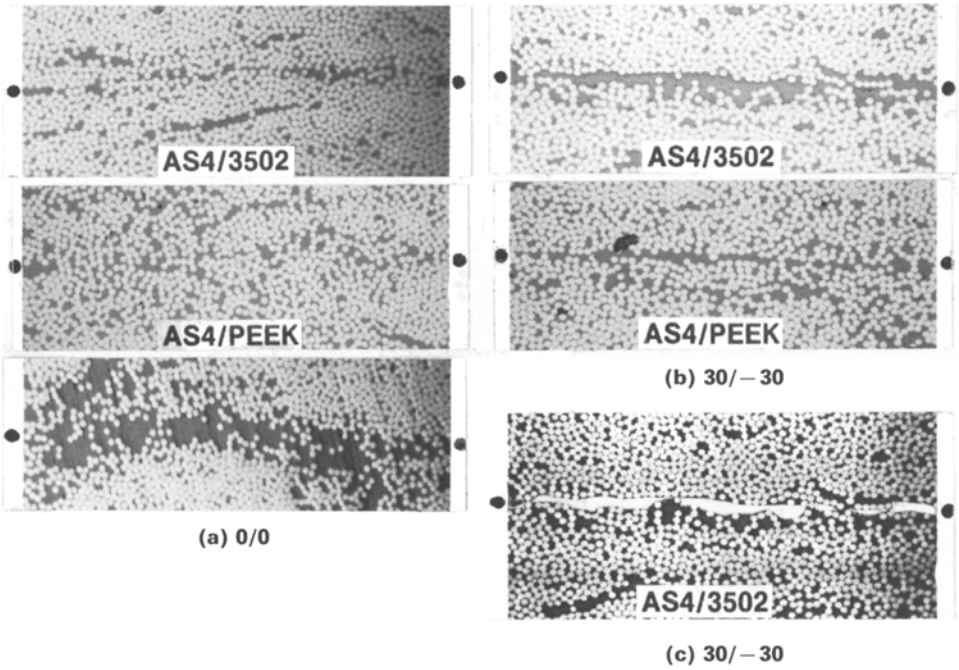

Fig. 10. Optical micrographs of polished transverse sections of composites. Solid circles at prints margin denote the delamination plane. Fiber diameter is 7.5 μm. (c) – Figurative description of the way the interlaminar resin layer thickness was determined; print shows the upper micrograph of (b) after isolation of the interlaminar resin layer.

resin-rich pockets smoothly around the fibers. The effective resin thickness, t_r, was determined by first producing a photomontage ($\times 300$) of the entire section of a given test specimen, cutting off the resin-rich region per Fig. 10c, and weighing it against a reference area. This was done for all interfaces except the 0/0 ones for AS4/3502 and AS4/PEEK where such procedure is obviously impractical. For these two cases, an analytic estimate was made by assuming a uniform type fiber distribution and by taking the shortest distance between the surfaces of two adjacent fibers, S, as t_r. Taking the fiber distribution to be the average result from a square and an hexagonal unit cell representation, one has from [16]

$$t_r \equiv S = d(0.92/\sqrt{v_f} - 1) \tag{3}$$

where v_f is the fiber volume fraction and d is the fiber diameter, measured to be 7.5 μm. Table 1 shows the analytic results obtained by assuming v_f in the resin rich zone to vary from 0.4 to 0.6 (the latter value is typical of the laminate average), and the experimental results as averaged from two independent measurements on each sample.

Figure 11 compares the interlaminar shear fracture energies from Table 1 with their adhesive bond counterparts, the latter were determined from Fig. 9 based on corresponding t_r values given in Table 1. The composites' G_{IIIC} is represented by both the "initiation" and "asymptotic" values. As shown in Fig. 11, the data for each test configuration are enclosed by a box whose horizontal dimension is dictated by the uncertainty in determining t_r. The adhesive and composite (whether "initiation" or "asymptotic") fracture energies seems

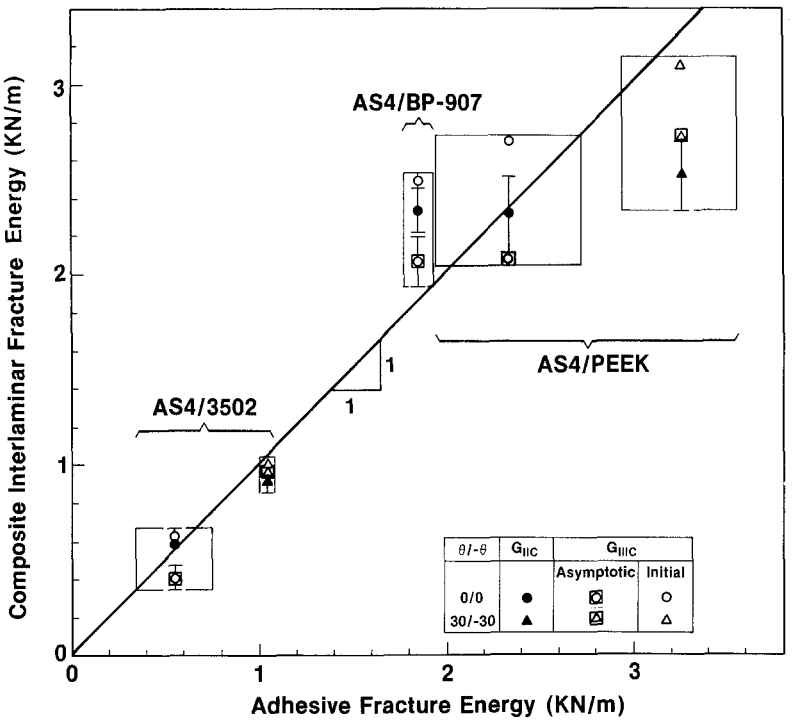

Fig. 11. Comparison of adhesive and interlaminar shear fracture energy. The mode III fracture energy of the composites is identified by both asymptotic and initial values. The adhesive fracture energy was determined from Fig. 9 based on the effective interlaminar resin thickness given in Table 1.

Table 1. Interlaminar fracture results*

Material	Delaminating interface	Mode II			Mode III			$t_r^{\dagger}$(μm)	G_{IIC} or G_{IIIC}(N/m) Adhesive joint‡
						G_{IIIC}(N/m)			
		N	M	G_{IIC}(N/m)	N	Asymptotic	Initiation		
AS4/3502	0/0	2	6	590(50)	3	410(130)	620(100)	1.4 – 3.4	340 – 750
	30/−30	3	3	915(55)	1	960	1005	4.8 ±0. 2	1040 ± 40
	60/−60	0			0				
AS4/BP-907	0/0	3	9	2325(240)	2	2065(255)	2485(55)	11.9 ± 0.6	1855 ± 75
	60/−60	0			0				
AS4/PEEK	0/0	3	7	2315(390)	2	2010(75)	2695(55)	1.4 – 3.4	1935 – 2730
	30/−30	2	2	2515(365)	2	2730(100)	3100(25)	4.8 ± 0.8	3245 ± 305

* The following nomenclature is used: N – total no. of specimens in which failure was truly interlaminar, M – corresponding no. of test data. Total no. of specimens tested for each type of delaminating interface was 3. Parentheses enclose standard deviation.

† Values measured experimentally except for 0/0 interface, AS4/3502 and AS4/PEEK, that were evaluated from (3).

‡ Determined from Fig. 9 based on the given t_r values.

to correlate well for all materials and delaminating interfaces. This, in turn, suggests that the difference in G_{IIC} or G_{IIIC} between the 0/0 and the off-axis interfaces for a given material is a mere consequence of differing resin enrichment in the interlaminar region.

A recent study concerning the effect of material processing on interlaminar fracture toughness of AS/3501-6 laminates shows that G_{IIC} is only marginally affected by the interlaminar resin layer thickness, the latter was varied by controlling the resin bleed during

cure [17]. For example, a change in t_r from 4.4 to 10 μm led to only a 20 percent increase in G_{IIC}. In contrast, Fig. 9 shows that a similar change in t_r for the H3502 epoxy leads to about 300 percent increase in adhesive fracture energy. Moreover, while G_{IIC} is quite fixed for $t_r > 10\,\mu$m, in [17] it was found to continuously increase for all given t_r values (i.e. up to 18 μm). Such discrepancies are quite unexpected giving the similarity between the two matrices under discussion and the good composite-joint correlation from Fig. 11. It is believed that this is due in part to the differing procedures used in evaluating the effective resin layer thickness.

After the submission of this paper for publication, the author became aware of a new finite-element analysis aimed at determining the distribution of the energy release rate components along the delamination front for the mode III specimen shown in Fig. 1b. This analysis revealed the existence of a mode II component, in addition to mode III, which tended to be maximized at the specimen edges. The relative magnitude of G_{II} was found to increase with increasing the ratio of crack length to beam width. For the slenderness ratio employed in this work or in [8] (i.e. $a/b \approx 10$), the overall contribution of G_{II} slightly exceeds that of G_{III}. Nevertheless, the coincidence of the results from the present "mode III" specimens with those of the pure mode II specimens do sustain our proposition that $G_{IIC} = G_{IIIC}$. In turn, the present "mode III" test is a valid test for measuring the shearing fracture toughness, G_{SC}.

5. Summary and conclusions

Testing and data reduction procedures for characterizing interlaminar shear fracture of laminated composites were developed which allowed for an unbiased assessment of the role played by the matrix on such failure. The finite width of the mode III specimen used in this study gives rise to a mixture of mode II and mode III energy release rates at the delamination front. However, this impurity is not critical inasmuch as $G_{IIC} = G_{IIIC}$. The interlaminar shear failure was associated with extensive resin plasticity as well as some microcracking at the crack tip region. The initial phase of damage development was followed by a self-similar crack growth. For mode III, the process of plastic deformations was accompanied by the development of an additional damage zone characterized by fiber bridging. The full extent of that zone was much larger than the plastic zone. Neglect or improper accounting of these effects seem to be the leading cause for the large scatter in published mode II and mode III interlaminar fracture data.

The "resistance" fracture behavior in mode III was probablistic, and its significance as a material characteristic is doubtful. In contrast, the initial value, evaluated at the instant of plastic zone maturity, was reproducible, associated with an interlaminar type morphology, and thus is proposed here as the true measure of G_{IIIC}. The so defined fracture toughness in mode III coincided with its mode II counterpart for all test configurations, which reinforce an earlier proposition from adhesive bonds that fracture is a phenomenon controlled by only two parameters, namely G_{IC} and G_{SC}. In contrast with commonly held viewpoints, morphological evidences suggest G_{SC} to be governed by plastic deformations at the crack tip vicinity, the contribution of hackles being marginal. In view of the good composite-joint correlation in Fig. 11, it is tempting to suggest that the zone of plastic deformations does not deviate appreciably from the interlaminar crack plane.

In accordance with earlier mode I results, the composites G_{SC} could be accurately predicted from a simple and economic, adhesive bond test provided the bondline thickness coincides with the effective thickness of the interlaminar resin layer. The results from the adhesive bond tests imply, in turn, a great sensitivity of G_{SC} to material processing variables affecting the size of the interlaminar resin layer. This was highlighted by the relatively large G_{SC} value for the present AS4/BP-907 composite that was attributed to an unusually thick interlaminar resin layer.

References

1. N.J. Johnston (ed.), *Toughened Composites, ASTM STP 937* (1987).
2. A.J. Russell and K.N. Street, in *Toughened Composites, ASTM STP 937* (1987) 275–294.
3. T.K. O'Brien, G.B. Murri and S.A. Salpekar, "Interlaminar Shear Fracture toughness and Fatigue Thresholds for Composite Materials," presented at *ASTM Conference on Composite Materials: Fatigue and Fracture*, Cincinnati, OH, April 28–30, 1987.
4. R.A. Jurf and R.B. Pipes, *Journal of Composite Materials* 16 (1982) 386–394.
5. E.A. Armanios, L.W. Rehfield and A.D. Reddy, *Composite Materials: Testing and Design, ASTM STP 893* (1986) 232–255.
6. L.A. Carlsson, J.W. Gillespie and B.R. Trethewey, *Journal of Reinforced Plastics and Composites* 5 (1986) 170–187.
7. W.M. Jordan and W.L. Bradley, in *Toughened Composites, ASTM STP 937* (1987) 95–114.
8. H. Chai, *International Journal of Fracture* 37 (1988) 137–159.
9. G.R. Sidey and F.J. Bradshaw, in *Carbon Fibers, Their Composites and Applications*, Proceedings of the International Conference of the Plastics Institute, London (1971) 208–213.
10. G.R. DeBaise, "Mechanics and Morphology of Wood Shear Fracture," Ph.D. thesis, State University College of Forestry, Syracuse University, New York (1970).
11. S.L. Donaldson, "Mode III Interlaminar Fracture of Composites", Master thesis, University of Dayton, OH (1987).
12. H. Chai, *Engineering Fracture Mechanics* 24 (1986) 413–431.
13. W.S. Johnson and P.D. Mangalgiri, *Journal of Composite Technology and Research* 9 (Spring 1987) 10–13.
14. J.D. Barrett and R.O. Foschi, *Engineering Fracture Mechanics* 9 (1977) 371–378.
15. H. Chai, *Composites* 15 (1984) 277–290.
16. D. Hull, *An Introduction to Composite Materials*, Cambridge Solid State Science Series (1981).
17. A.J. Russell, *Polymer Composites* 8 (1987) 342–351.
18. R.H. Martin, NASA TM 101562 (1989).

Résumé. On a étudié la rupture par décollement en mode II et en mode III de plusieurs composites évolués, en utilisant des éprouvettes en forme de barreaux et la microscopie électronique à balayage.

Un accent particulier a été placé sur la solution d'aspects liés au matériau, portant sur le processus de rupture et sur la quantification des effets de la matrice sur l'énergie de rupture.

On a trouvé que l'énergie de rupture en mode II est indépendante de la longueur de fissuration tandis que, pour le Mode III, elle fait état d'un comportement de "résistance" de caractère plutôt probabilité, attribué à l'effet de pontage entre les fibres.

L'énergie d'amorçage de la rupture, que l'on considère ici comme la vraie mesure de G_{IIIC}, coïncide avec G_{IIC}.

Pour les deux modes de sollicitation, la région de séparation en avant de l'extrémité de la fissure fait état d'une déformation plastique importante, dont on pense qu'elle contrôle sérieusement la ténacité due composite.

L'énergie de rupture entre couches en cisaillement, que l'on appelle ici G_{SC} ($= G_{IIC} = G_{IIC}$), a pu être prédite avec exactitude par des essais de rupture de joints collés, pour autant que l'épaisseur de l'adhésif coïncide de avec celle de la couche de résine entre deux plans du colaminé.